Irreversible diffusion-limited cluster aggregation: The behavior of the scattered intensity

Francesco Sciortino, Andrea Belloni, and Piero Tartaglia

Dipartimento di Fisica, Università di Roma La Sapienza, Piazzale Aldo Moro 2, I-00185 Roma, Italy

In this paper, we discuss the evolution of the scattered intensity $I(q)$ during irreversible diffusion-limited cluster-cluster aggregation. We propose a mean field model to describe the correlation among different clusters that develops during the irreversible aggregation process. The model is based on two coupled differential equations, controlling the growth of the average cluster mass and the time dependence of the probability of finding pairs of clusters as a function of their distance. The model predicts a moving and growing peak in the scattered intensity at a wave vector q_m. For growing compact clusters, as in the case of late-stage decomposition under deep-quench conditions, we recover the expected results both for the scaling law of the scattered intensity, i.e., $q_m^d I(q/q_m) = f(q/q_m)$, and for the growth of the average cluster mass. For growing clusters with fractal dimension D_f, the model predicts no scaling for $I(q)$, particularly in the initial stage of the aggregation. Only in the late stages, an approximate scaling of the scattered intensity in $q_m^{D_f} I(q/q_m)$ holds. We compare the prediction of the model with the recent experimental results of Carpineti and Giglio [Phys. Rev. Lett. **68**, 3327 (1992)] on colloidal aggregation and with data from Brownian dynamics simulations. The agreement between analytical and experimental results is excellent.

PACS number(s): 82.70.Dd, 64.60.Cn, 05.40.+j

I. INTRODUCTION

The process of supramolecular ordering, like the growth of the minority phase in unstable binary mixtures or the growth of crystalline regions in a supercooled system [1,2], is characterized in Fourier space by a wave vector q and time t dependent scattered intensity $I(q,t)$. The shape of $I(q,t)$ and its evolution during the aggregation process convey information on the leading aggregation mechanism [3–6]. For this reason, a considerable interest, both theoretical and experimental, has been dedicated to the determination of $I(q,t)$ for several supramolecular ordering processes in the last decades [3,4]. Often $I(q,t)$ is characterized by a well defined peak at the wave vector q_m. During the growth process, the growth of the aggregates in mass and radius manifests itself in the growth of the peak amplitude and in the shift of the peak position toward smaller and smaller wave vectors. The scattered intensity at different times can sometime be scaled on a common master curve by plotting $q_m^d I(q/q_m)$ versus q/q_m [3], suggesting an underlying scaling in space and time of the ordering process.

Cluster-cluster aggregation phenomena have also been studied extensively, both theoretically and experimentally, in the last decades. The simplest nontrivial cluster aggregation model is the so-called diffusion-limited cluster-cluster aggregation (DLCA) [7]. DLCA describes a process of irreversible aggregation among noninteracting freely diffusing clusters. When two different diffusing clusters touch each other, they aggregate. The newly formed cluster continues to diffuse. DLCA has been shown to generate clusters whose average mass $\langle M \rangle$ grows with time as t^z and whose bell-shaped cluster size distribution scales in time. Differently from the decomposition case, DLCA clusters are fractals. None of the extensive studies on DLCA had focused on the spatial arrangement of the growing clusters, except for a (not well known) suggestive but unsatisfactory one-dimensional theory [8]. Not one of the several old computer simulations of the DLCA model was ever scrutinized for the existence of a characteristic length scale in the cluster-cluster spatial arrangement, the real space analogue of the scattered intensity peak. It came thus as a big surprise the finding of Carpineti and Giglio, three years ago, that the experimentally measured scattered intensity in diffusion-limited cluster aggregation does display a peak, which grows and shifts in q space during the aggregation kinetics. Carpineti and Giglio found that after an initial regime, the measured scattered intensity seems to scale exactly as predicted for late-stage decomposition theories, if one substitutes the fractal dimension of the clusters D_f to the space dimension d in the scaling plot. The growth of the scattered intensity stops when the less and less dense fractal clusters completely fill the available space, leaving in the frozen scattered intensity state a memory of the growth process.

The experimental observation of Carpineti and Giglio [9] were confirmed by the following experimental studies on cluster-cluster correlation in two-dimensional systems [10] and by computer simulations [11–14]. Even in the two-dimensional case, a growing and moving peak in the scattered intensity is observed. From the available real-space images and from mass conservation [9,2,10], it was conjectured that the peak was a manifestation in Fourier space of the the depletion region, which develops around the growing clusters. The description of the spatial and time extent of such a depletion region, and the way it

manifests itself in Fourier space, is the main point of this paper. A preliminary paper was presented in Ref. [15]. Here we give a more complete description of the theory and analyze a variety of effects of cluster geometry, initial monomer concentration, etc., on the observed development of the depletion zone.

The theory we present in this paper applies not only to cluster-cluster aggregation kinetic, but also to ordinary late-stage decomposition in the deep-quench limit, i.e., when the cluster structure is compact and the leading aggregational mechanism is diffusion and coalescence of clusters. We propose an analytic form for the structure factor and for its kinetic evolution as a function of the starting droplet density, highlighting the common features between late-stage spinodal decomposition and cluster-cluster aggregation.

II. THEORY

Before formally introducing the equations that describe the evolution of the scattered intensity, it is worthwhile to examine a pictorial representation of the system and its evolution during DLCA aggregation, as modeled via two-dimensional computer simulations of DLCA. Figure 1 shows three snapshots, at different times, of a two-dimensional Brownian dynamics simulation of freely diffusing particles undergoing irreversible aggregation. The top row shows the simulated system, while the bottom row is an enlarged portion of the same configurations, to visualize the fractal nature of the cluster structure.

From Fig. 1, one sees that clusters are surrounded by empty spaces, appearing during the aggregation. The sequence of full and empty spaces introduces a characteristic length, which can even be picked by the eyes in the top row of the figure. We also note that the clusters have roughly the same size, in agreement with the bell-shaped form of the cluster size distribution. On increasing the time, the size of the cluster increases but the structure of the alternating regions with different density is preserved.

To describe quantitatively the cluster-cluster correlation observed in Fig. 1, we study the time evolution of the mass concentration $c(r, t)$ at distance $r > 2R(t)$ from the origin, knowing that one cluster of mass $M(t)$ and radius $R(t)$ is at the origin. In agreement with the basic ingredients of the DLCA model, we assume that (i) $c(r, t)$ changes only via cluster diffusion, i.e.,

$$\frac{\partial c(r, t)}{\partial t} = D \nabla^2 c(r, t). \tag{1}$$

D is the diffusion coefficient of a cluster of mass M relative to the cluster fixed at the origin. We assume D to be mass dependent $(D = 2D_0 M^{-\gamma})$. (ii) The mass concentration at $r = 2R(t)$ is zero, as imposed by the irreversible aggregation, i.e., $c(2R(t), t) = 0$. (iii) The growth of the cluster at the origin satisfies mass conservation. The mass growth is controlled by the mass flux at the moving boundary $2R(t)$, the sum of the radii of the two coalescing clusters, i.e.,

$$\frac{dM}{dt} = D \left(S_d \frac{\partial c(r, t)}{\partial r} \right)_{2R(t)}, \tag{2}$$

where S_d is the surface term, equal to 2, $2\pi r$, $4\pi r^2$ for $d = 1, 2, 3$, respectively. Radius and mass of the average cluster are related via $(R(t)/R(0))^{D_f} = M(t)/M(0)$, allowing the study of the equations for compact $(D_f = d)$ as well as for fractal clusters. To completely define the system of Eqs. (1) and (2), we chose as initial and boundary conditions $c(r, 0) = c_0, r \geq 2R(0)$ and $c(\infty, t) = c_0$, reflecting the initial homogeneous state and the absence of correlation between very distant clusters. $c(r, t)$ is by definition the product of the number density $n(r, t)$ times the average mass $M(t)$ [16]. Expressing Eqs. (1) and (2) in terms of $n(r, t)$, we obtain
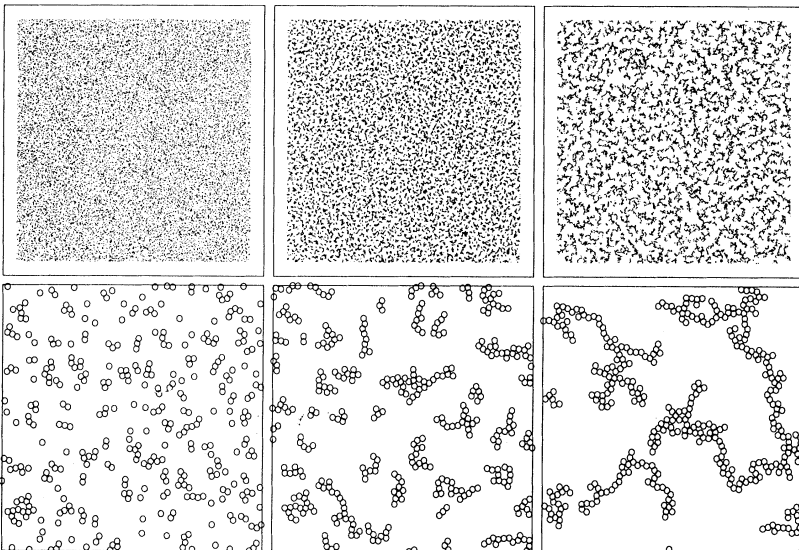

FIG. 1. Top row: Three different snapshots of a two-dimensional system of 32 000 particles undergoing diffusion-limited cluster aggregation. Clusters are allowed to diffuse and rotate with a diffusion coefficient proportional to the inverse of the mass. The initial volume fraction is 0.013. The bottom row shows the same data on a ten times bigger scale, to highlight the cluster structure.

$$\frac{\partial n}{\partial t} = D\nabla^2 n - \frac{n}{M}\frac{dM}{dt}, \qquad (3)$$

$$\frac{dM}{dt} = DM\left(S_d \frac{\partial n}{\partial r}\right)_{2R(t)}, \qquad (4)$$

with boundary conditions $n(2R, t) = 0$ and $n(\infty, t) = n_0 M(0)/M(t)$, and initial conditions $n(r, 0) = n_0$ for $r \geq 2R(0)$ [16]. By comparing Eqs. (3) and (4) with Eqs. (1) and (2), one notes that $c(r, t)$ changes only via diffusion, while changes in $n(r, t)$ are controlled by the usual cluster diffusion process and by changes in the number of clusters produced by the aggregational process.

Before analyzing the solutions of the model, we stress that the description of the aggregation process proposed is in terms of average quantities. The average mass is a good candidate for the description of the aggregation process only when the cluster size distribution is quasimonodisperse. This condition is not fulfilled in the reaction-limited regime, in the DLCA regime at very high initial monomer concentration, as well as in the initial stage of DLCA aggregation when the memory of the initial monodisperse distribution is not yet lost. To deal with such cases, the model has to be extended to take into account the polydispersity. Such work is underway.

A. Compact clusters

Aggregation of compact clusters is particularly relevant in the case of late-stage spinodal decomposition in the limit of deep quenches, when a sample is quickly transferred from the high temperature one-phase region deep into the coexistence region. After an initial period during which droplets of the minority phase are formed, the separation process proceeds via diffusion and clustering of droplets. Under deep quench, separation proceeds only along a path of decreasing total energy and cluster breaking is very rare. In such conditions, mechanisms like the evaporation condensation are less effective than the mechanism of diffusion and coalescence of the entire clusters, which we study here.

In the case in which the cluster structure is compact (i.e., $D_f = d$), $n(r, t)$ and $M(t)$ can be calculated exactly by performing a change of variable $s = D_0 t^{2/(2+\gamma d)}$, corresponding to writing $ds = D(M)dt$, and noting the analogy with the so-called moving boundary Stefan problem [17]. The solution is a function of the scaled variable $r/(2s^{\frac{1}{2}})$ [18],

$$n(r, s) = \begin{cases} n_0 \frac{M(0)}{M(s)}\left[1 - \frac{F(r/(2s^{\frac{1}{2}}))}{F(\lambda)}\right], & r \geq 2R(s) \quad (5) \\ n(r, s) = 0, & r \leq 2R(s). \quad (6) \end{cases}$$

$F(x)$ is given by

$$F(x) = \begin{cases} \text{erfc}(x), & d = 1 \quad (7) \\ \text{Ei}(-x^2), & d = 2 \quad (8) \\ \frac{e^{-x^2}}{x} - \sqrt{\pi}\text{erfc}(x), & d = 3. \quad (9) \end{cases}$$

The associated solution for the boundary motion is

$$R(s) = \lambda s^{1/2}. \qquad (10)$$

λ depends only on the ratio Φ between the initial solution density and the density of the growing cluster. λ is obtained by inserting the solution for $n(r, s)$ and $R(s)$ in Eq. (4) and solving the resulting equation. For $d = 1$, 2, and 3, respectively, λ is given by the solution of the following relations:

$$\sqrt{\pi}\text{erfc}(\lambda)\lambda e^{\lambda^2} = \Phi, \quad d = 1, \qquad (11)$$

$$\text{Ei}(-\lambda^2)\lambda^2 e^{\lambda^2} = -\Phi, \quad d = 2, \qquad (12)$$

$$2\lambda^2 e^{\lambda^2}[e^{-\lambda^2} - \lambda\sqrt{\Pi}\text{erfc}(\lambda)] = \Phi, \quad d = 3. \qquad (13)$$

The growing cluster acts as a trap for the near clusters, decreasing the probability of finding clusters nearby its sticky boundaries. The scaling properties of the solution show that plots of $n(r, s)M(s)$ versus $r/s^{0.5}$, or by virtue of Eq. (10) versus $r/R(s)$, for different s values will collapse on a single master curve. We also note that Eqs. (3) and 4 satisfy mass conservation at all times. The mass that was contained in the depletion region at $t = 0$ coincides with the mass of the growing cluster, or in terms of number density

$$\int [n(r, s) - n(\infty, s)]d\mathbf{r} = -1 \qquad (14)$$

for all s values. Thus, for a fixed mass of the growing cluster, the size of the depletion region will be larger the smaller the initial density. This is shown in Fig. 2, which displays the scaling function $n(r, s)M(s)$ versus r/R for three different initial monomer densities in the $d = 3$ case. The analytic solution of the model also shows that the growth of the radius of the average Euclidean cluster is controlled by the same exponent as the growth of the depletion region. The fact that the same scaled variable controls both radius and size of the depletion
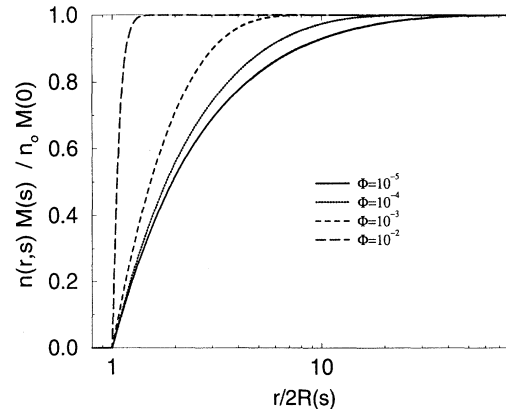

FIG. 2. Scaled number density $n(r, s)$ as a function of $r/R(s)$ in three dimensions for four different values of the ratio Φ between the initial solution density and the density of the growing cluster. Note that when the density of the initial solution is small, the size of the depletion region is large.

region already suggests that the system is characterized by only *one* characteristic length.

To make contact with the experimental results, we look next to the behavior in Fourier space. $n(r,t)$ is by definition the product of the average number density times the radial distribution function [19]. The associated cluster structure factor is [19]

$$S(q,s) = 1 + \int [n(r,s) - n(\infty,s)]e^{i\mathbf{q}\cdot\mathbf{r}}d\mathbf{r}. \quad (15)$$

At small q, we can expand the exponential term in the right-hand side of Eq. (15) in a series. By using Eq. (14) and symmetry considerations, we see that the leading term in the small q expansion is q^2, as imposed by mass conservation. Moreover, being $n(r,s)$ a function of the scaled variable $r/2s^{\frac{1}{2}}$, also $S(q,s)$ scales in time in $qs^{1/2}$ or, by Eq. (10), in $qR(s)$. The total scattered intensity $I(q,t)$ measured experimentally can be approximated as the product of the previously calculated $S(q,t)$ and of the so-called cluster form factor $P(q,t)$, a well known function for any d [20]. $P(q,t)$ takes into account the intracluster contribution to the scattered intensity. Only in absence of correlation among clusters, $I(q,t) \sim P(q,t)$, being $S(q,t) = 1$. $P(q,t)$ can be expanded at low q as $P(q,t) \sim M(t)(1 - R_g^2 q^2/3)$, and at high q values as $P(q,t) \sim q^{-(d+1)}$, where R_g is the gyration radius of the cluster. $P(q,t)$ is proportional to the mass of the scatterer, i.e., in our case to the mass of the average cluster and it is a function only of qR, i.e., of the same scaled variable of $S(q,t)$. This implies that the total scattered intensity will also be a scaled function of qR and that a plot of $I(qR(t))/M(t)$ versus $qR(t)$ will show a remarkable data collapse, of the same kind as observed in late-stage spinodal decomposition [3]. From the limiting behavior of $S(q,t)$ and $P(q,t)$, we have that at low q, the total scattered intensity goes as q^2, being controlled by $S(q)$, while at high q it goes as $q^{-(d+1)}$, being fixed by the decay of the form factor for objects with sharp interfaces. It is important to note that $P(q,t)$ does not depend on the number of clusters in solution at any time. Thus, differently from $S(q,t)$, $P(q,t)$ is independent from the initial number density n_0. As a consequence, the scaling function for $I(q,t)$ will depend on n_0. The smaller the initial number density, the larger the depletion region and the smaller the q vector at which a maximum in the scattered intensity will occur. On lowering the initial monomer concentration, the $I(q,t)$ maximum will eventually move out from the finite experimental window [21].

From the solution of the differential equations, we also calculate the value of the exponent z, controlling the power-law growth of the mass. On going from s to t and using $M \sim R^d$, we find $M(t) \sim t^{\frac{d}{2+\gamma d}}$. In three dimensions and with the $\gamma = 1/d$ value for Stoke-Einstein diffusion, we recover the Smoluchowski result $z = 1$. It is worthwhile stressing that the $z = 1$ value was obtained by Smoluchowski using a time independent aggregation probability. It is also worth observing that the $M(t)$ dependence we find is the same obtained from the Binder-Stauffer diffusion-reaction mechanism for droplet coars-

ening [22], without imposing any *ad hoc* requirement of self-similarity in the droplet configuration.

B. Fractal clusters

It is known that the growth of fractal clusters is limited in time and space. Fractal clusters tend to fill the space, being characterized by an average density, which decreases with the cluster size, i.e.,

$$\rho(r) = \rho_0 (r_0/r)^{d-D_f}, \quad (16)$$

where ρ_0 and r_0 are, respectively, the density scale constant and the monomer radius. When clusters reach a space filling configuration, gelation occurs. One single cluster fills up all the available space. When the growing cluster is a fractal, a new length scale related to the average cluster size at the gelation point is expected to arise. The change in time of the average cluster density complicates the structure of Eq. (4). The relation between mass and radius gives now $dM \sim R^{(D_f-1)}dR$, an R dependence that does not cancel any longer the surface term in the right-hand side of Eq. (4). This extra R dependence reflects the fact that the radius grows faster than it would if D_f were equal to d. On the other end, the diffusion of the fractal clusters is still happening on an Euclidean substrate, so that no change in the characteristic space-time relations are expected in the evolution of the depletion region. The changes in the time dependence of the cluster growth compared to the time dependence of the growth of the depletion region, brings as a consequence that the $n(r,t)$ profile does not scale anymore with $R(t)$. Figure 3 shows the numerical solution of Eqs. (3) and (4) in the case $d = 3$ and $D_f = 1.9$ at different times. Differently from the compact cluster case, $M(s)n(r,s)$ versus r/R is now a function of time.
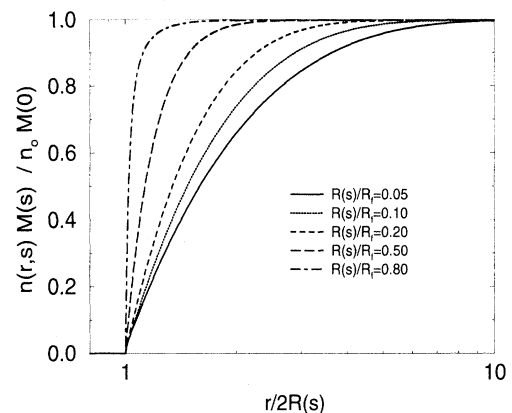

FIG. 3. Scaled number density $n(r,s)$ as a function of $r/R(s)$ calculated solving numerically Eqs. (3) and (4) in the case of $D_f = 1.9$ and $d = 3$. Differently from the previous figure, the different curves refer to the same system but at different stages of the aggregation process. Note that the density profile $n(r,s)$ becomes similar to a step function at long times, when $R(s)$ approaches R_f.

The decrease in average density of the growing clusters requires a depletion region profile, which progressively approximates a step function. In different words, while in the compact case doubling the radius of the growing cluster requires a doubling of the size of the depletion region; in the fractal case, the size of the depletion regions has to increase less than two times the cluster radius, because the average cluster density is also reduced.

On increasing the time, the intercluster distance becomes comparable with the cluster size. In this late-stage regime, the profile of $n(r)$ becomes very similar to a step function and the cluster radius appear to be the only typical length scale. Under such circumstances, which appear close to gelation, an apparent scaling in $qR(t)$ is again expected. The numerical solution of the equations shows also that during the initial stage of the growth process, (when the intercluster distance is much bigger than the cluster size) the flux of matter at R is proportional to R^{d-2}, as in the Euclidean case. Under such conditions, from Eq. (4) one has $R^{D_f-1}dR/ds \sim R^{d-2}$, which immediately gives R going as $s^{\frac{1}{D_f-d+2}}$ or $M \sim t^{\frac{D_f}{D_f(1+\gamma)-(d-2)}}$, the classical mean field exponent [7]. When the intercluster distance becomes comparable to the cluster size, the numerical solution of the equations shows a faster and faster increase of the average mass, which diverges when the average density of the fractal cluster becomes equal to the initial monomer density.

Before comparing the prediction of the theory with numerical and experimental results, we note that the model we propose can be expressed in the case of fractal growing clusters in terms of a scaled variable $x = r/R_f$, where R_f is defined as the radius of the cluster at gelation. R_f depends only on the parameters in Eq. (14) and on the monomer concentration at $t = 0$. We define R_f via

$$\rho_\infty(2R_f)^d = \int_{r_0}^{R_f} \rho_0(r_0/r)^{d-D_f}r^{d-1}dr, \qquad (17)$$

where ρ_∞ is the density of the sample at $t = 0$. The important point is that it is possible to recast Eqs. (3) and (4) in the scaled variable $x = r/R_f$

$$\frac{\partial n^*}{\partial t} = D^*\nabla_x^2 n^* - \frac{n^*}{M}\frac{dM}{dt}, \qquad (18)$$

$$\frac{dM}{dt} = D^*M\nabla_x n^*|_{2X(t)}, \qquad (19)$$

where $D^* = D/R_f^2$, $X(t) = R(t)/R_f$, and $n^*(x,t)$ is a dimensionless number density. The corresponding initial and boundary conditions become $n^*(x,0) = 1$ and $n^*(\infty,0) = 1$. The initial monomer density now appears in the equations only through R_f. Thus, the model predicts that at constant ratio $R(t)/R_f$, one should observe the same scattering pattern, independently of n_0. This brings as a consequence that the scaling form of the total scattered intensity in the gel state should be the same independently from the initial monomer density, a prediction that has been recently confirmed experimentally [23].

III. COMPARISON WITH SIMULATION RESULTS

In this section we compare the predictions of the model with Brownian dynamics (BD) simulations. The comparison with simulations results is particularly valuable because it allows testing the cluster-cluster correlation in real and Fourier space as well as the approximation of the total scattered intensity as a product of the form factor times the structure factor. We have performed simulations only in one and two dimensions. Simulations in three dimensions of comparable size are still too demanding from a computational point of view.

A. One dimension

We report in this section results in one dimension. We have performed simulations in one dimension because this offers the possibility of studying the aggregation process both for compact and for fractal aggregates as shown in the following. We simulate coagulating systems of N monomer of length one on a $d = 1$ continuum of length L. The initially monodisperse distribution of monomers is allowed to evolve in time performing BD, with time step 0.01. At each step, touching clusters are joined irreversibly to form a new cluster of mass equal to the sum of the old masses and length equal to the sum of the length of the previous clusters to the power $1/D_f$. In such a way, the fractal dimension of the clusters can be fixed to any chosen value. D has been kept constant [$D(M) = 1$] for simplicity. We report here the results for two different simulations, one with $D_f = d = 1$, $N = 10^5$, and $L = 10^6$, and one with $D_f = 0.5$, $N = 5 \times 10^4$, and $L = 25 \times 10^6$. In both cases, we observe that the cluster size distribution evolves toward a bell-shaped scaled function of the average cluster size, confirming that one characteristic mass is present at each time. This is a particularly relevant issue, being one of the basic ingredient of the model proposed in the previous section.

We calculate the structure factor $S_{\rm BD}(q,t)$, the cluster form factor $P_{\rm BD}(q,t)$, and the total scattered intensity $I_{\rm BD}(q,t)$ from the simulation, according to the following equations [24]:

$$I_{\rm BD}(q,t) = \frac{1}{N}\left\langle \left|\sum_{i=1}^{N} e^{i\mathbf{q}\cdot\mathbf{r}_i(t)}\right|^2\right\rangle, \qquad (20)$$

$$S_{\rm BD}(q,t) = \frac{1}{n_c(t)\langle M^2\rangle}\left\langle \left|\sum_{k=1}^{n_c(t)} m_k e^{i\mathbf{q}\cdot(\mathbf{r}_{\rm c.m.k}(t))}\right|^2\right\rangle, \qquad (21)$$

$$P_{\rm BD}(q,t) = \frac{1}{N}\left\langle \sum_{k=1}^{n_c(t)}\left|\sum_{i=1}^{m_k} e^{i\mathbf{q}\cdot\mathbf{r}_i(t)}\right|^2\right\rangle, \qquad (22)$$

where $r_i(t)$ is the position of the ith monomer, $r_{\rm c.m.k}(t)$ and m_k are, respectively, the center of mass and mass of cluster k, and $n_c(t)$ is the number of clusters at time

t. The $n(r,t)$ function has been determined by calculating all the center of mass cluster-cluster distances and weighting each pair in the distribution with the product of the cluster masses.

Figure 4 shows the comparison between the theoretical predictions, Eqs. (5)–(10) and the simulation results for the time dependence of the average mass and of the cluster number density $n(r,t)$. The left column describes the case $D_f = 1 = d$ and the right column $D_f = 0.5 \neq d$. Figure 5 shows the form factor, the structure factor, and the total scattered intensity for the same simulations. In the compact case, the high q limit is q^{-2} as predicted by a sharp one-dimensional interphase, while it goes as q^{-D_f} in the fractal case. The scaled form factors shown in the first row in Fig. 5 have been used, together with the $S(q,t)$ quantities calculated according to Eqs. (5) and (15) to obtain the theoretical total scattered intensity data shown as lines in the last row. As predicted by Eq. (5), the $n(r,t)$ and $S(q,t)$ data obtained from the simulation collapse on the same curve once plotted as a function of the scaled variable $qR(t)$ or $r/R(t)$ for the $D_f = d$ case, while no scaling is observed for the truly fractal case. The agreement is excellent, especially if one considers that there are no adjustable parameters. A few considerations are in order: (i) The theory predicts very well not only the initial stage of aggregation, but also the gelation transition, shown in the steep increase of the average mass versus time in Fig. 4. (ii) The form factor has a high q behavior equal to $q^{-2} = q^{-(d+1)}$ in the compact case and $q^{-0.5} = q^{-D_f}$ in the fractal case. Below $qR = 1$, the scaled form factor is almost constant and

equal to $\langle M^2 \rangle / \langle M \rangle^2$. (iii) The structure factor at low q goes as q^2. $S(qR)$ is almost a constant equal to one for $qR > 1$. (iv) The total scattered intensity is well reproduced by the product of the form and structure factor. $P(q)$ controls the high q behavior, while $S(q)$ is responsible for the low q part of $I(q)$, as shown in Fig. 6. (v) The normalization of the $F(q)$ factor is given by the average mass. Superposition of the high q part of the total scattered intensity [which as we said before is controlled by $P(q)$] can only be achieved scaling the x axis by the inverse of a length and the y axis by the same length to the D_f power.

The low q behavior of the total scattered intensity predicted by our model is q^2 due to mass conservation. Differences from the q^2 behavior can be observed in simulations and in real experiments at very high volume fraction and/or in the initial stage of the aggregation. Indeed, the theory we proposed does not take into account the possibility of initial thermal fluctuations in the monomer distributions, which contribute with a background to $I(q)$. If the average cluster size is small, then the contribution to the scattered intensity at low q may become comparable to the signal arising from the depletion region, hiding the q^{-2} behavior. For very high volume fractions, when the average size of the cluster close to the gelation point is very small, the thermal background could also strongly affect the overall scaling of the scattered intensity. Simulations are very valuable in showing this effect, because they allow comparison of the development of the total scattered intensity peak with different starting conditions. The left side of Fig. 7 shows the low q
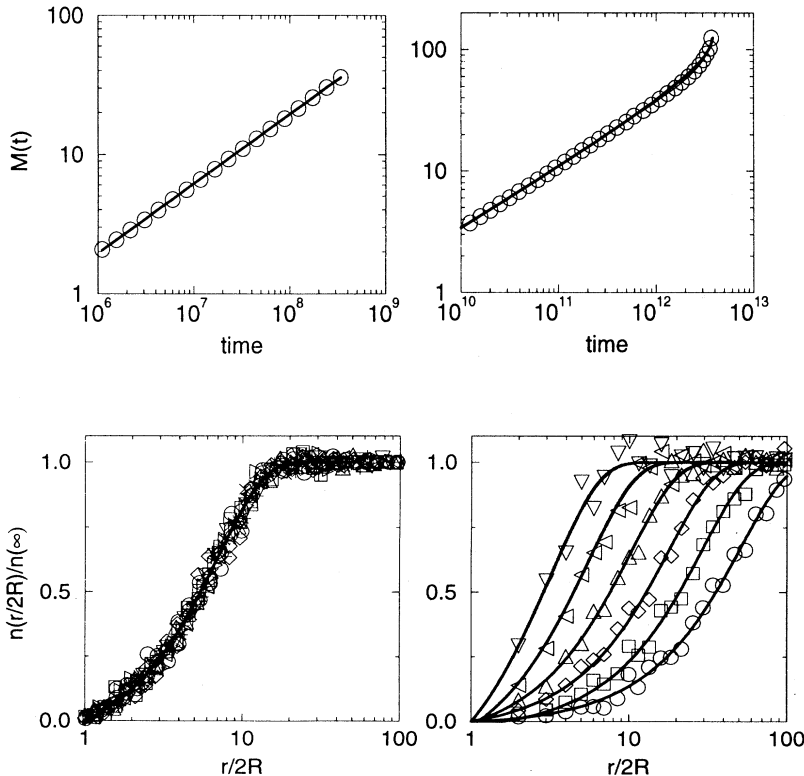

FIG. 4. Average mass as a function of time (top) and scaled number density $n(r,t)/n(\infty,t)$ as a function of $r/2R(t)$ for different times (bottom). The full lines are the predictions of the model while symbols are results from the one-dimensional Brownian dynamics simulation. The left column refers to compact growing clusters, the right column to fractal ($D_f = 0.5$) clusters. Note the scaling in $n(r,t)$ in the case of compact growing clusters

behavior of $I(q)$, calculated from a BD simulation having a random distribution of nonoverlapping monomer as the initial configuration. The right side of the same figure shows the same quantity calculated from a BD simulation having a regular array of monomer as the initial state. In both cases, $I(q)$ at $t = 0$, shown in open symbols, is compared with $I(q)$ when the average cluster size is about six (filled symbols). As shown in the figure, the low q^2 behavior may be completely masked by the initial thermal fluctuations if the signal coming from the aggregation process is not much larger than the initial thermal scattering.

B. Two dimensions

We have performed also two-dimensional Brownian dynamics to simulate a coagulating systems of $N = 32\,000$ monomers of diameter one for different densities. This monodisperse distribution of monomers is allowed to evolve in time performing BD, with scaled time step $2D_1\delta t = 10^{-4}$, where D_1 is the diffusion coefficient of the monomer. At each step, touching clusters are joined irreversibly to form a new cluster. Clusters are allowed to translate and rotate as rigid objects with translational and diffusional coefficient scaling with mass as $D(M) = D_1 M^{-1}$. We have observed that for such choice of γ, the cluster size distribution evolves toward a bell-shaped scaled function of the average cluster size, confirming that one characteristic mass is present at each time. Figure 8 shows the behavior of the gyration radius as a function of the cluster mass at three different concentrations. At high concentration ($\Phi = 0.3$), the fractal dimension is $D_f = 1.65 \pm 0.05$; while at the two lower concentrations ($\Phi = 0.06$ and $\Phi = 0.03$) simulated systems $D_f = 1.42 \pm 0.20$ in agreement with previous estimates [7]. Figures 8(b) and 8(c) show the cluster growth dynamics. At the higher concentration the dynamics is
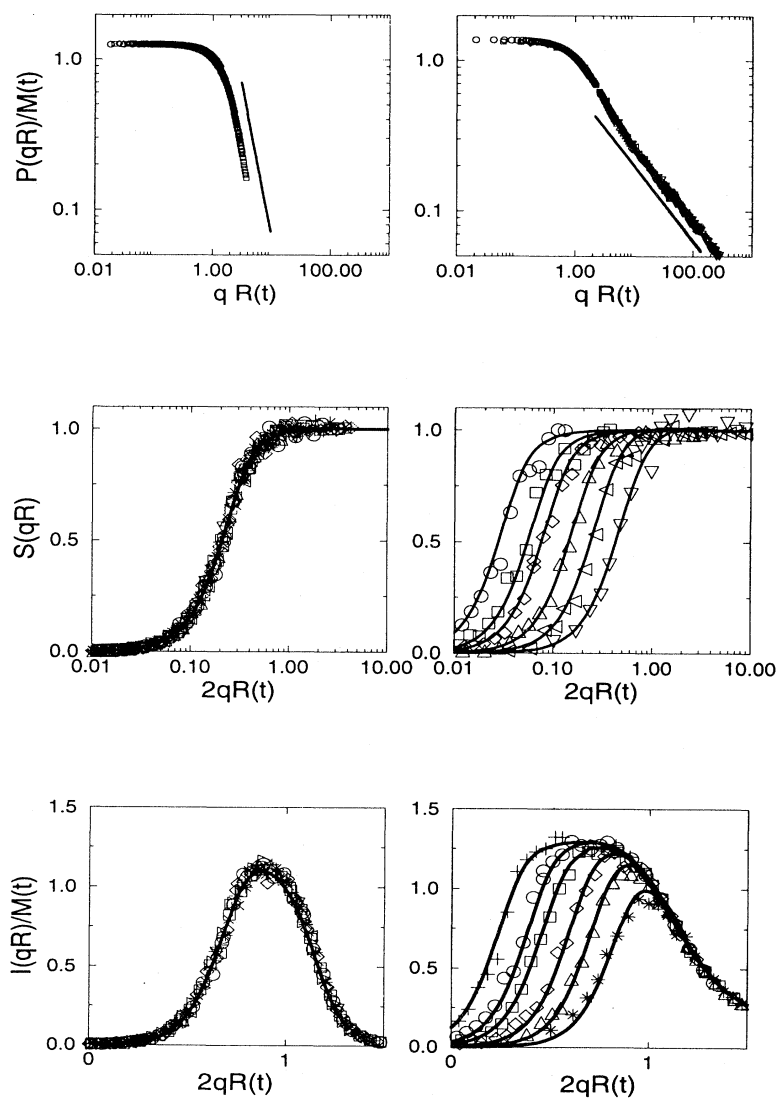

FIG. 5. Form factor $P(q)$ (top), structure factor $S(q)$ (center), and total scattered intensity $I(q) = P(q)S(q)$ from the simulation as a function of qR for the compact (right column) and fractal (left column) case. Symbols are from the simulation. Full line for $S(q)$ and $I(q)$ are derived from the model. $P(q)$ and $I(q)$ are scaled by the mass. Note that $P(0,t)/M(t)$ is slightly bigger than one, due to the presence of a small polydispersity. Polydispersity has been taken into account in the theory increasing the cluster density in the analytical solution by $\langle M^2 \rangle / \langle M \rangle^2$.
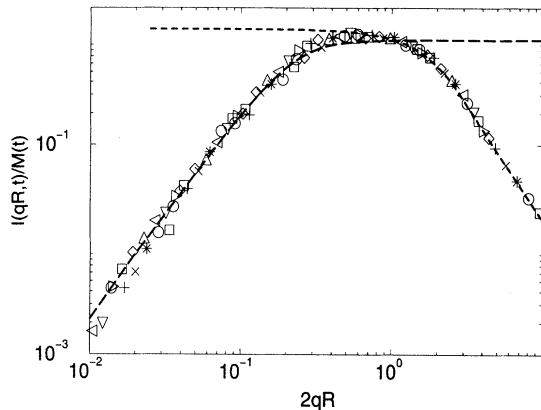
FIG. 6. Log-log plot of the scaled total scattered intensity as a function of the scaling variable qR for the compact cluster case in $d = 1$. Symbols are from the BD simulation described in the text, lines are the analytic solutions for $S(q)$ and $P(q)$. Note the predicted power-law behaviors at small and high q values as well as the role respectively played by $S(q)$ and $P(q)$ at small and high q wave vectors.

very fast, the mass growth is not a simple power law, and the size distribution is not characterized by just one single size, as shown by the growing ratio of the first two moments of the size distribution function. At lower concentrations, $M(t) - M(0) \sim t^z$ in the early stages and then crosses over to a faster growth law on approaching
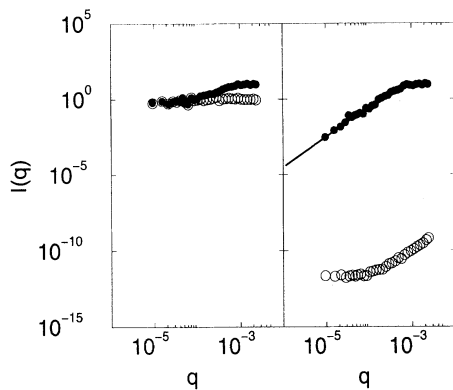

FIG. 7. Total scattered intensity for two different samples differing in the initial configuration. Left: $I(q)$ for a thermally equilibrated system, at $t = 0$ when the average mass is one (open symbols) and when the average mass is five (filled symbols). Right: Same quantities but for a system prepared originally in an ordered configuration. The line has a slope two. Note the very low scattering at small q vectors at $t = 0$ in the second case, a reflection of the absence of spatial fluctuations in concentration in the initial configuration. The figure shows that the q^2 behavior, which characterizes the aggregation process can be masked by the initial thermal fluctuations. This is particularly true during the very early stage of aggregation (when the cluster mass is not much bigger than one) or in very concentrated samples for which the average cluster size at gelation is very small.

the gelation point. z is slightly concentration dependent and equal to about 0.6 at $\Phi = 0.03$. When $M(t)$ ceases to grow as t^z, the ratio of the first two moments of the size distribution function starts to increase.

Symbols in Fig. 9 are total scattered intensities for $\Phi = 0.3$ and $\Phi = 0.03$ at two different times. The lines in Fig. 9 are the product of the form factor times the structure factor as evaluated from Eqs. (21) and (22). The data in Fig. 9 show that (i) there is a peak in the scattered intensity at all concentrations. At high concentration, the amplitude of the peak is rather small, consistent with the fact that just before gelation, the average cluster size is small. (ii) The total scattered intensity is well represented by the product of $P(q)$ and $S(q)$ only at low density. This reflects the fact that at $\Phi = 0.3$ the kinetics of aggregation never enters the regime of self-similarity. The cluster distribution changes shape with time, as shown in Fig. 8(b) and it is still polydisperse. The aggregation process is so fast that there is no time to forget the initial monodisperse distribution state and crossover to the universal law for the cluster size distribution. At lower densities, the kinetics is much slower, and indeed $I(q)$ is well described by $S(q)P(q)$.

Figure 10 shows the numerical solution of Eqs. (3) and (4) in the case $d = 2$ and $D_f = 1.4$ at different times. Differently from the compact cluster case, $c(r, t)$ versus $r/2R$ is a function of time. The decrease in average density of the growing clusters requires a depletion region profile, which progressively approximates a step function. On increasing the time, the intercluster distance becomes comparable with the cluster size. In this late-stage regime, the profile, of $c(r, t)$ becomes very similar to a step function and the cluster radius appears to be the only typical length scale. When the intercluster distance becomes comparable to the cluster size, the numerical solution of the equations shows a faster and faster increase of the average mass, which diverges when the average density of the fractal cluster becomes equal to the initial monomer density. The time dependence of the average mass is reported in Fig. 10(b). As found from the BD simulations, at high initial densities, the average mass growth is not described by a power law; while at low initial density, a well defined region exists in which $M(t) \sim t^z$. The exponent z derived from the theory increases slowly with concentration, starting from $z = 0.58$ at $\Phi = 0.0001$, in full agreement with the simulation results.

Figure 11 shows the comparison between the theoretical $c(r, t)$ function (lines) and the same quantity evaluated from the BD simulation in the case of $\Phi = 0.03$ (symbols) for two different times. $c(r, t)$ from the BD data has been determined by calculating all the center of mass cluster-cluster distances and weighting each distance by the product of the cluster masses. Figure 11(b) shows the structure factor and the form factor at the same times, evaluated according to Eqs. (21) and (22). We note that while the form factor data do scale in the scaled $qR(t)$ variable, the $S(q)$ data do not. This means that the total scattered intensity, which is given by the product of $P(q)$ and $S(q)$, will not scale in $qR(t)$. Also, the low q behavior of $S(q)$ is given by q^{-2}, as imposed by
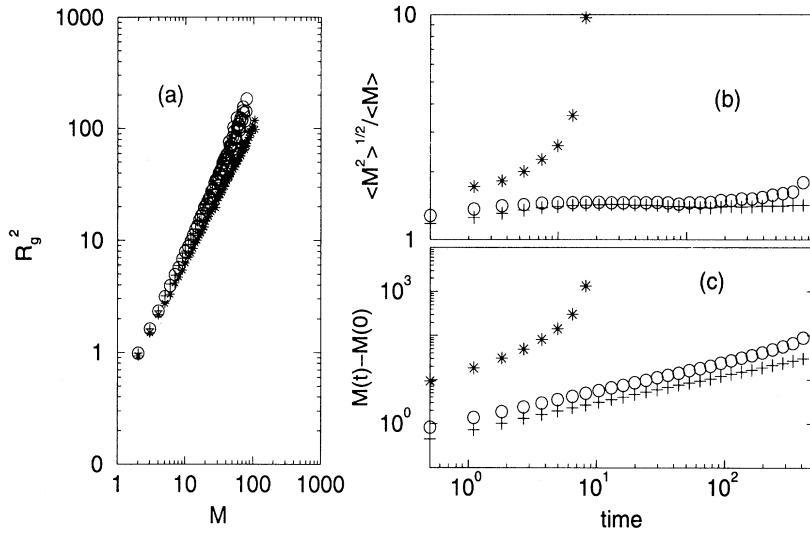
FIG. 8. Results from the BD simulation in two dimensions. (a) Average gyration radius as a function of cluster mass. Clusters have been divided in different bins according to their mass. R_g^2 has then been calculated for each of such bin. The * are the $\Phi = 0.3$ simulation, + are $\Phi = 0.06$, and o are $\Phi = 0.03$. (b) The ratio of the first two moments of the cluster size distribution. Symbols are the same as in (a). (c) The average mass as a function of time for the three concentrations studied.

mass conservation. We also note that the low q behavior can be masked by the presence of trivial thermal fluctuations, fluctuations also found in the nonaggregated system (i.e., at $t = 0$). The signal from the thermal fluctuations becomes negligible only when the aggregation process has gone so far to produce a large ($\gg 1$) average mass.

The scattered intensity shows a well defined peak that moves in time. The kinetic process is separated in three regions: an initial region where no scaling in $q_m^{D_f} S(q/q_m)$ is observed (symbols in Fig. 12), an intermediate region where scaling is observed (symbols in Fig. 13), and a saturation region where no further change in the dynamical structure factor is observed. On the basis of experimen-

IV. COMPARISON WITH EXPERIMENTAL RESULTS

We compare now the predictions of our model with the experimental results of Carpineti and Giglio [9] on aggregation of polystyrene spheres in water. They observed the formation of clusters with $D_f \approx 1.9$ for $d = 3$.
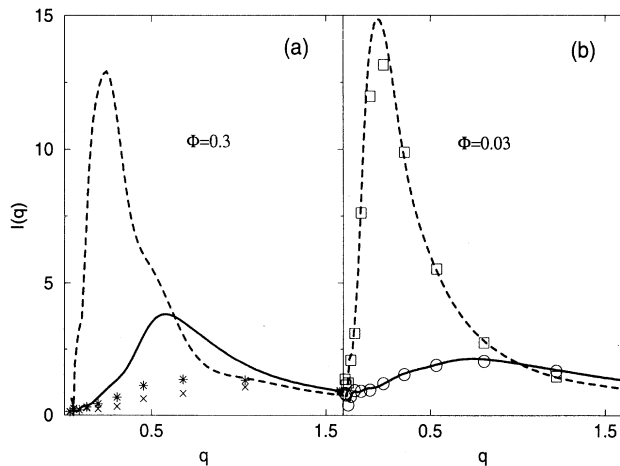

FIG. 9. (a) Symbols: Total scattered intensity at two different times [$t = 1.1$ (x) and $t=3.7$ (*)] at $\Phi = 0.3$. Lines: $P(q)S(q)$ for the same configurations. (b) The same for $t = 4.9$ (o) and $t=340$ ($\square$) but at $\Phi = 0.03$. Note that in this case $I(q)$ is very well represented by $P(q)S(q)$.
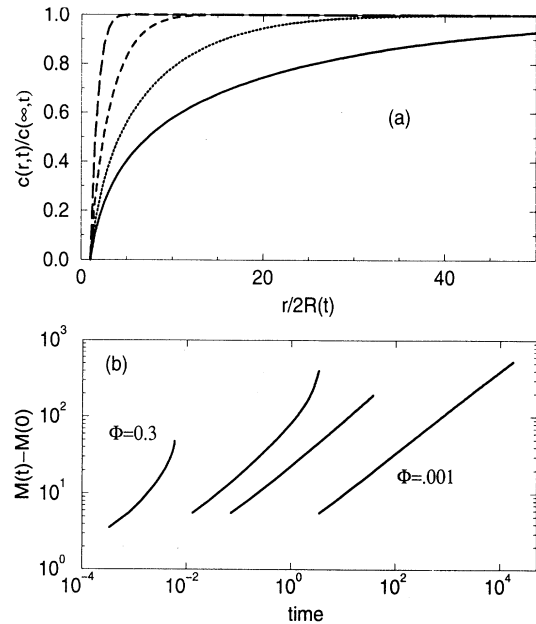

FIG. 10. (a) Scaled number density $c(r,t)/c(\infty,t)$ as a function of $r/2R(t)$ calculated solving numerically Eqs. (3) and (4) in the case of $D_f = 1.4$ and $d = 2$. The different curves show the density profile for different times, increasing from right to left. Note that the density profile $c(r,t)$ becomes similar to a step function at long times. (b) The average mass as a function of time for some of the concentrations studied: $\Phi = 0.3, 0.06, 0.02,$ and 0.001.
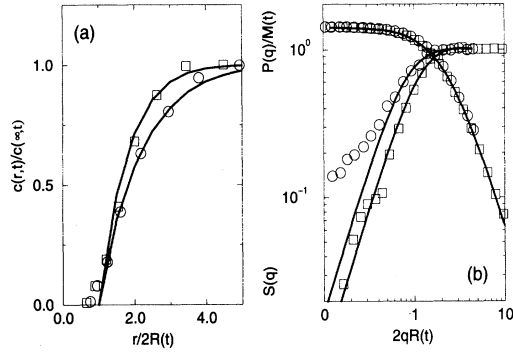
FIG. 11. (a) $c(r,t)$ for $D_f = 1.4$ in $d = 2$ at two different times. Symbols are from the BD simulation at $t = 19.7$ (o) and $t = 409$ ($\square$), full lines are from the theory at the corresponding times. (b) $S(q)$ and $P(q)/M(t)$ from the simulation [symbols are the same as in (a)] and from the theory (full lines) as a function of $2qR(t) = qM(t)^{-1/D_f}$. Note the bending of $S(q)$ at small q for the $t = 19.7$ case, when the thermal fluctuations are comparable with the scattering from the (still small) aggregates. Note also that while the form factors can be scaled in $qR(t)$, the structure factor, depending on the time development of the depletion region, does not scale in $qR(t)$. The total scattered intensity, given by the product of $I(q)P(q)$ obviously does not scale.

tal work, it is not possible, of course, to know the radius growth law to scale data in qR as we have done in the previous section. For this reason, experiments are presented in q/q_m, q_m being the experimentally determined position of the maximum in the total scattered intensity. To make contact with the experimental work, we present our data also in q/q_m, even if as shown later on in this section, such a choice may obscure the absence of true scaling for growing fractal clusters discussed in the previous sections.

We have calculated $S(q,t)$ from the numerical solution of Eqs. (3) and (4) with $D_f = 1.9$. For $P(q,t)$, we use a
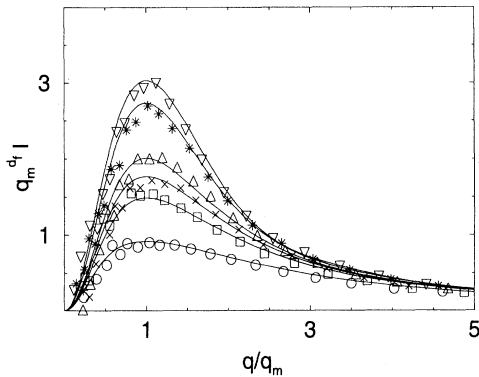

FIG. 12. Comparison between experiments and theory in the $d=3$ case: scaled $I(q,t)$ at different times during the aggregation process in the *nonscaling* regime. Symbols are experimental data redrawn from [9]. The full lines are the prediction of the model.
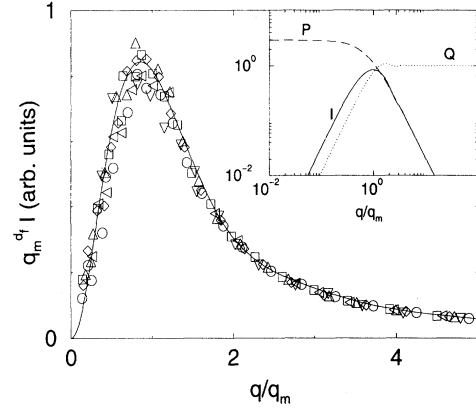

FIG. 13. Comparison between experiments and theory in the $d=3$ case: Scaled $I(q,t)$ at different times during the aggregation process in the *scaling* regime. Symbols are redrawn from [9]. The full line is the prediction of the model when the $n(r)$ function can be approximated with a step function. The inset shows $I(q)$, $S(q)$, and $P(q)$ in log-log scale to highlight the q^2 and the $q^{-1.9}$ behavior as well as the contribution of $P(q)$ and $S(q)$ to $I(q)$.

standard Fisher-Burford equation [25] ,

$$P(q) = \frac{P(0)}{[1 + (qR_g)^2]^{D_f/2}}, \qquad (23)$$

relating the gyration radius R_g in this expression to $R(t)$ according to $R_g^2 = (3 - D_f + d)/(5 - D_f + d)[R(t)]^2$. Equation (23) has been shown to give a satisfactory representation of the experimental cluster form factor [26]. The validity of Eq. (23) is limited to q vectors smaller than the inverse of the monomer size, above which one should observe the scattering arising from the monomer form factor. The experimental data that we compare with are well within the region of validity of Eq. (23). The volume fractions studied in the experiments range between 3×10^{-5} and 3×10^{-3}, supporting the possibility of writing $I(q)$ as a product of $S(q)$ and $I(q)$.

The total scattered intensity, $I(q,t) = S(q,t)P(q,t)$ at selected times in the nonscaling regime is shown in Fig. 12 and compared with the data from Ref. [9]. In the scaling region the scaled $q_m^{d_f} I(q/q_m)$ are within a few percent coincident with the $q_m^{d_f} I(q/q_m)$ obtained approximating $n(r,t)$ with a step function. The growth of the cluster in this time region produces significant changes of $n(r,t)$ in real space, but only very minor changes in the normalized $n(r/R,t)/n(\infty,t)$ function. In this region, an apparent scaling of $q_m^{d_f} I(q/q_m)$ has again been observed, being the size the depletion region very close to the cluster radius. The final $q_m^{d_f} I(q/q_m)$, calculated assuming a step function shape for $n(r,t)$, and Eq. (23) for the form factor, is compared with the experimental data [9] in the scaling regime in Fig. 13. The agreement between the experimental data and the prediction of Eqs. (3) and (4 is surprisingly good, both in the nonscaling and in the scaling regions.

We now come back to the topic of apparent scaling in $I(q)$ observed in experiments. On the basis of our analytical calculation, we can calculate q_m exactly for all times, and obtain the theoretical $q_m^{d_f} I(q/q_m)$ behavior. The result of such calculations in the pregelling regime is shown in Fig. 14. The left panel shows the unnormalized and unscaled $I(q,t)$ functions; the central panel of Fig. 14 shows the correctly normalized $q_m^{d_f} I(q/q_m)$ versus q/q_m; the right panel shows the same data plotted as $q_{bm}^{d_f} I(q/q_{bm})$ versus q/q_{bm}, where q_{bm} is defined as the best q values to obtain a fictitious scaling. The apparent scaling observed in the right panel is made possible by using a q_{bm} value only a few percent different from the true q_m, which, as shown in the central panel, would not give a true scaling. Differences between q_m and q_{bm} are well within the experimental errors. This may explain why close to gelation the experimental uncertainties in the position of the maximum have suggested the presence of apparent scaling. In the late-stage regime, the apparent scaling allows the calculation of the z exponent from the experimental data, being $I(q,t) \sim M(t)$. The calculated value is $z = 1$ [9], consistent with the prediction of our model, when for γ the hydrodynamic regime value $1/D_f$ is chosen.

Before concluding this section, we stress that the presence of a peak in the scattered intensity is independent from the initial monomer density. The initial density only modulates the position in q space at which the peak will appear. For very diluted concentrations, the depletion region is so large that the peak appears well below the experimental resolution of light scattering experiments. On increasing concentration, the initial position of the $I(q,t)$ peak will move to higher q values. This explains why the peak in $I(q,t)$ was only detected when fairly concentrated samples were investigated.
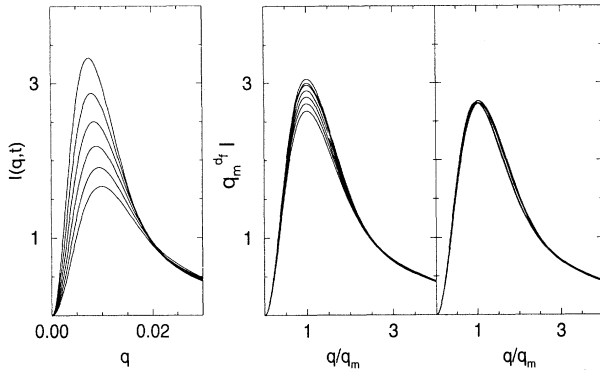

FIG. 14. Theoretical $I(q,t)$ for $D_f = 1.9$ in $d = 3$ in the pregelling regime [$R(s)/R_f = 0.56, 0.62, 0.68, 0.75, 0.83, 0.91$, and 1.0]. The same data are plotted as $q_m^{D_f} I(q/q_m)$ in the central panel and as $q_{bm}^{d_f} I(q/q_{bm})$ in the right panel. q_m is the position of the maximum of $I(q)$. q_{bm} has been chosen as the "best" q to maximize the agreement in the scaling form. q_{bm} is only a few percent different from the true q_m value. The apparent scaling shown in the right panel is well within the experimental error. This may explain why close to gelation the experimental uncertainties in the position of the maximum have suggested the presence of apparent scaling.

V. CONCLUSIONS

In summary, we have discussed in detail a simple model [15] to describe the origin and the development of the spatial correlatations among clusters during DLCA. The origin of the correlation is ascribed to the formation of a depletion zone around the growing clusters [2]. From the model, we have calculated the dynamic exponents controlling the time dependence of the average mass and of the radius of the aggregates, obtaining the same exponents predicted by the Smoluchowski equations [27]. Differently from the Smoluchowski equations, no a priori evaluation of the reaction rates kernels is required, but only information on the dimension of the growing cluster. We have also calculated the scattered intensity and its evolution during the aggregation process. We have shown that a peak in $I(q,t)$ arises as a manifestation in Fourier space of the existence of a depletion zone around the growing clusters. The model shows that $I(q,t)$ truly scales, during the whole aggregation process, only for compact growing clusters where correlations have the same scaling behavior as the size of the growing cluster. In both quantities, distance scales with reduced time s as $s^{\frac{1}{2}}$. Under such conditions, the $I(q,t)$ can be scaled as $I(qR,t) \sim M(t)F(qR) \sim [R(t)]^d F(qR)$. The function $F(qR)$ is not universal, but depends on the difference in density of the cluster compared to the bulk density.

When the growing cluster is a fractal, as in DLCA, the theory predicts an absence of scaling in the time development of the scattered intensity. The reason for such a difference is shown to arise from the different time scale of $R(t)$ and $n(r,t)$. While cluster growth is controlled by the fractal dimension, the mass diffusion is still controlled by the dimensionality of the space in which diffusion takes place. Only close to gelation, when clusters are very close, the growth of the cluster takes over the diffusional process and an apparent scaling is observed. In this limit $I(qR,t) \sim [R(t)]^{d_f} F(qR)$. Differently from the compact cluster case, the $F(qR)$ function is independent of the initial monomer density, a prediction that has been recently experimentally confirmed [23]. Samples with different initial monomer concentration are predicted to show the same scattering pattern if compared at the same R/R_f value.

The theory we propose here only allows us to study processes where a typical cluster size does exist and it is not thus immediately extended to the early DLCA stages, to DLCA in high concentration regimes, and to reaction-limited cluster-cluster aggregation (RLCA). This notwithstanding, we do expect in the RLCA regime that the presence of an activation energy for aggregation, which would reflect in our model in the modification of the boundary conditions from sticky to partially adsorbing [28], will cause a significant increase in the size of the depletion region and the squeezing of $S(q,t)$ toward $q = 0$. On moving from DLCA toward RLCA, the $I(q)$ peak position will thus shift toward smaller and smaller q values, eventually moving out from the available experimental window. Such behavior has been recently observed [21,10]. Work in this direction is underway.

The colloidal aggregation process discussed in this pa-

per, which leads to to formation of a gellike state in which fractal clusters fill up the available space, is followed by a much slower process of spatial reorganization of the clusters. Such a slow process, very hard to study experimentally in three dimensions due to the simultaneous presence of the sedimentation process, seems to produce an increase of the cluster fractal dimension. There is evidence, both from experiments and simulations, that the slow local arrangement of the monomers leads to the formation of ordered microcrystalline structures. The q vector range in which the signal coming from the microcrystalline ordering would appear is beyond the range studied in this article.

Before concluding, we note that irreversible aggregation in the compact cluster case is strongly related to the phase separation problem. Indeed, irreversible aggregation can be seen as a phase separation process in the deep-quench limit (from infinite to zero temperature), when separation proceeds only along a path of decreasing total energy and cluster breaking is very rare. In such conditions, mechanisms like the evaporation condensation are less effective than diffusion and coalescence of the entire clusters. The $M(t)$ dependence we find is the same obtained from the Binder-Stauffer diffusion-reaction mechanism for droplet coarsening [22], without imposing any *ad hoc* requirement of self similarity in the droplet configuration. The q^2 and q^{-4} limit in $I(q,t)$ in the late-stage decomposition in the deep quench also coincides with the $I(q,t)$ behavior during aggregation predicted by our model in three dimensions. Our exact results support the view that the scaling function is not universal and depends strongly on the initial conditions and coarsening process.

ACKNOWLEDGMENTS

[1] K. Schatzel and B.J. Ackerson, Phys. Rev. Lett. **68**, 337 (1992).

[2] G.P. Banfi, V. Degiorgio, A.R. Rennie, and J.G. Barker, Phys. Rev. Lett. **69**, 3401 (1992).

[3] For a general review on spinodal decomposition see, e.g., J.D. Gunton, M. San Miguel, and P.S. Sahni, in *Phase Transition and Critical Phenomena*, edited by C. Domb and J.L. Lebowitz (Academic Press, New York, 1983), Vol. 8, p. 267.

[4] H. Furukawa, Adv. Phys. **34**, 703 (1985).

[5] I.M. Lifshitz and V.V. Slyozov, J. Phys. Chem. Solids **19**, 35 (1961).

[6] M. Tokuyama and Y. Enomoto, Phys. Rev. E **47**, 1156 (1993).

[7] For a general review see, e.g., T. Vicsek, *Fractal Growth Phenomena* (World Scientific, Singapore, 1989); P. Meakin, in *The Fractal Approach to Heterogeneous Chemistry*, edited by D. Avnir (Wiley, New York, 1989); several articles in *On Growth and Form*, edited by H.E. Stanley and N. Ostrowsky (M. Nijhoff Publishers, Dordrecht, 1986); D.A. Weitz and M. Oliveria in *Kinetics of Aggregation and Gelation*, edited by F. Family and D.P. Landau (North-Holland, Amsterdam, 1984).

[8] J. A. Marqusee, Phys. Rev. A **35**, 1856 (1987).

[9] M. Carpineti and M. Giglio, Phys. Rev. Lett. **68**, 3327 (1992).

[10] D.J. Robinson and J.C. Earnshaw, Phys. Rev. Lett. **71**, 715 (1993)

[11] P.N. Pusey, A.D. Pirie, and W.C. Poon, Physica A **201**, 322 (1992); M. D. Haw, W.C.K. Poon, and P.N. Pusey, *ibid.* **208**, 1 (1994).

[12] F. Sciortino, A. Belloni, and P. Tartaglia, Nuovo Cimento **16D**, 1159 (1994).

[13] T. Sintes, R. Toral, and A. Chakrabarti (unpublished).

[14] A.E. Gonzales and G. Ramirez-Santiago, Phys. Rev. Lett. **74**, 1238 (1995).

[15] Preliminary results about this model have been recently published in F. Sciortino and P. Tartaglia, Phys. Rev. Lett. **74**, 282 (1995).

[16] The cluster fixed at the origin does not contribute to $n(r,t)$. For this reason, $n(r,t) = 0$ for $r < 2R$.

[17] J. Crank, *The Mathematics of Diffusion* (Oxford University Press, New York, 1956); H.S. Carlslaw and J.C. Jaeger, *Conduction of Heat in Solids* (Oxford University Press, New York, 1959).

[18] The solutions are valid for $R(0) = 0$ or when $R(t) >> R(0)$.

[19] J.P. Hansen and I.R. McDonald, *Theory of Simple Liquids* (Academic Press, London, 1986).

[20] Such approximation is valid at low density and neglecting polydispersity.

[21] M. Carpineti and M. Giglio, Phys. Rev. Lett. **70**, 3828 (1993).

[22] K. Binder and D. Stauffer, Phys. Rev. Lett. **33**, 1006 (1974).

[23] M. Carpineti, M. Giglio, and V. Degiorgio, Phys. Rev. E **51**, 590 (1995).

[24] Quantities in Eqs. (21) and (22) are defined consistently with $S(q,t)$ of Eq. (15) to take into account the point nature of the scatterers and the presence of polydispersity.

[25] M.E. Fisher and R.J. Burford, Phys. Rev. **156**, A583 (1967).

[26] D. Asnaghi, M. Carpineti, M. Giglio, and M. Sozzi, Phys. Rev. A **45**, 1018 (1992).

[27] M. von Smoluchowski, Phys. Z. **17**, 557 (1916).

[28] G.H. Weiss, *Aspects and Applications of the Random Walk* (Elsevier Science, Amsterdam, 1994).